Journal of Applied Physics

RESEARCH ARTICLE | SEPTEMBER 03 2020

Mid-IR photothermal measurement of substantial heat transport by surface waves of polar amorphous films supported on silicon

S. Hamyeh; R. Tauk; P.-M. Adam; M. Kazan

J. Appl. Phys. 128, 095105 (2020)
https://doi.org/10.1063/5.0015577

AIP Publishing

Journal of Applied Physics ARTICLE scitation.org/journal/jap

Mid-IR photothermal measurement of substantial heat transport by surface waves of polar amorphous films supported on silicon

Cite as: J. Appl. Phys. **128**, 095105 (2020); doi: 10.1063/5.0015577
Submitted: 29 May 2020 · Accepted: 18 August 2020 ·
Published Online: 3 September 2020 · Corrected: 14 September 2020

S. Hamyeh,[1,2,3] R. Tauk,[2] P.-M. Adam,[3] and M. Kazan[1,a)]

AFFILIATIONS

[1]Department of Physics, American University of Beirut, P.O. Box 11-0236, Riad El-Solh, Beirut 1107-2020, Lebanon
[2]Platform for Research in Nanoscience and Nanotechnology, Faculty of Sciences 2, Lebanese University, Fanar Campus, P.O. Box 90239, Jdeidet 1202, Lebanon
[3]Light, Nanomaterials and Nanotechnology, University of Technology of Troyes, CNRS ERL 7004, 10004 TROYES, France

[a)]**Author to whom correspondence should be addressed:** mk140@aub.edu.lb

ABSTRACT

We present measurements of significant thermal diffusivity by surface electromagnetic waves of an ultra-thin polar and amorphous dielectric film deposited on silicon (Si). We used a photothermal-beam-deflection technique with a modulated mid-infrared heating source to excite and launch surface electromagnetic waves onto the surface of an amorphous silicon carbide (a-SiC) film deposited on Si and generate periodic temperature and refractive index gradients above the sample surface. These gradients are capable of periodically deflecting a probe beam, passing very close to the surface, at the modulation frequency of the heating beam. We have fitted the measured probe beam deflection to an analytical model for the mirage effect that takes into account the thermal anisotropy of the measured sample to infer the contribution of the surface electromagnetic waves of the a-SiC film to thermal diffusivity in the plane of the sample under study. We found that reducing the thickness of the a-SiC film promotes the interaction between the surface electromagnetic waves propagating on either side of the a-SiC film, which significantly enhances thermal diffusivity in the plane of the measured sample. We also found that in-plane thermal diffusivity by surface electromagnetic waves on an amorphous silicon carbide film a few nanometers thick is several orders of magnitude greater than thermal diffusivity by phonons in silicon. We believe that the results obtained provide a better understanding of the physics of electromagnetic waves confined to solid surfaces.

I. INTRODUCTION

The increased need for lab-on-a-chip tools and integrated nanoelectronics has led to a reduction in the size of electronic components to a length of a few tens of nanometers. Technology industries expect an even smaller size for these components soon. This continuous reduction in the size of electronic components and the increase in their speed and frequency of operation inevitably leads to hot spots, which are hazards that may lead to system failure. Therefore, thermal management has become an increasingly pressing issue and a hot topic in microelectronics. While many research groups have demonstrated effective phonon engineering methods to reduce the thermal conductivity of dielectric materials for thermoelectric applications,[1–4] there is still a lack of practices regarding heat dissipation from low-dimensional dielectric materials in which conventional heat carriers (phonons) suffer from high scattering rates.

The interaction between energy-carrying electromagnetic waves and optical phonons in a polar material gives rise, under certain conditions, to *p*-polarized surface phonon-polariton (SPhP) waves, which are electromagnetic waves localized on the surface of the material.[5–7] Tunneling of the SPhP modes between polar dielectrics separated by a vacuum gap of a width not exceeding a few micrometers has shown orders of magnitude enhancement of thermal radiation in the near-field limit.[8–16] From a theoretical

perspective, SPhP modes can also transport heat by conduction and would meet the industrial need for highly efficient heat carriers in materials. Due to their long propagation length, long lifetime, shallow penetration depth, and electromagnetic character, SPhP modes are insensitive to the conventional scattering centers and, therefore, can carry an intense heat flux. Thermal conduction by SPhP modes is particularly noticeable in an ultra-thin polar dielectric film where the surface modes of one surface of the film interact with those of the other surface.[17–20] Moreover, as the thickness of the polar dielectric film decreases, the mean-free-path of the anti-symmetric SPhP modes of small wavevectors increases considerably, resulting in a further increase in the SPhP heat flux.[17]

Experimental studies have confirmed the theoretical predictions of efficient heat conduction by SPhP modes in suspended structures.[21–24] Temperature measurements of the surfaces of glass microtips provided a presumption of energy transport by SPhP modes,[22] and thermal excitation of SPhP modes followed by direct measurements of thermal conductivity of silicon dioxide (SiO_2) nanoparticles in various surrounding materials showed significant thermal conduction by SPhP modes at temperatures slightly above room temperature.[23] As for planar geometries, recent measurements have shown that in 20 nm thick suspended silica films maintained at room temperature, thermal conduction by SPhP modes is as efficient as thermal conduction by vibration modes.[24]

However, near-field measurements have shown that the inclusion of a polar dielectric film between two different non-polar mediums of positive dielectric constants results in remarkable confinement of SPhP modes to the surfaces of this film.[25–27] Such highly confined SPhP modes would have the potential to transport heat more efficiently than the SPhP modes of suspended polar films. In this paper, we study the in-plane thermal diffusivity by SPhP modes highly confined to the surfaces of an amorphous silicon carbide (a-SiC) film between a silicon (Si) substrate and the air. Using a photothermal-beam deflection technique with a mid-infrared (MIR) heating source, we were able to excite and launch SPhP modes confined to the surfaces of a-SiC films of different thicknesses and generate periodic temperature and refractive index gradients above the surface of the measured sample. These gradients are capable of periodically deflecting a probe beam, passing very close to the sample surface, at the modulation frequency of the heating beam. Then, we fitted measured probe beam deflections to an analytical model for the mirage effect that takes into account the thermal anisotropy of the measured sample to derive the in-plane thermal diffusivity of the sample as a function of a-SiC film thickness. The measurement results presented in this paper show the effect of the thickness of the a-SiC film (which determines the strength of the interaction between the waves propagating on either side of the a-SiC film) on thermal diffusivity by highly confined SPhP modes.

The choice of an amorphous polar dielectric film is beneficial in the present study for two reasons. First, it allows us to exclude thermal transport by phonons and electrons in the film and to observe the contribution of the SPhP modes to in-plane thermal diffusivity. Second, due to the high damping factor, the solution to the dispersion relations of the SPhP modes in the amorphous materials extends from $q = 0$ to $q \to \infty$ (where q is the wavevector), and, unlike crystals, there is no physical reason for excluding any part of it.[5] Hence, the large number of SPhP modes in amorphous materials allows a significant contribution of these modes to in-plane heat transport, although the broad imaginary parts of the infrared dielectric functions of the amorphous materials reduce the lifetimes and mean-free-paths of the SPhP modes whose frequencies are close to the vibration resonance frequencies.

II. EXPERIMENTS

We deposited thin a-SiC films on commercial Si (100) substrates by ablating a high purity SiC polycrystalline target under a background pressure of 10^{-6} mbar using a focused high power KrF excimer laser, with keeping the Si substrate temperature at 400 °C to ensure amorphization of the deposited films. We have grown three a-SiC films on Si with deposition times of 5 min, 15 min, and 40 min to obtain a-SiC films of different thicknesses. Surface measurements by atomic force microscopy (AFM) showed that the resulting films were 3 nm, 16 nm, and 40 nm thick. We present in Fig. 1 the Raman spectrum of the 40 nm thick a-SiC film on Si. The broad peak at 1456 cm^{-1} is a clear signature of amorphous Si_xC_{1-x} with $x = 0.5$.[28]

We used an MIR photothermal-beam-deflection experiment to evaluate the contribution of surface electromagnetic modes to thermal diffusivity in the sample plane. Readers can find a detailed description of the experimental setup in Ref. 29. We present in Fig. 2 the schematic diagram describing the fundamental characteristics of the measurement technique as well as the mechanisms of excitation and launching of SPhP modes on the surface of the measured sample. We also illustrate the detection of thermal waves generated in the air using the bending of the probe beam due to multiple refraction mechanisms in the air known as the mirage effect.

An acousto-optic modulator modulates a p-polarized 10.6 μm wavelength CO_2 laser beam focused on the sample surface. In

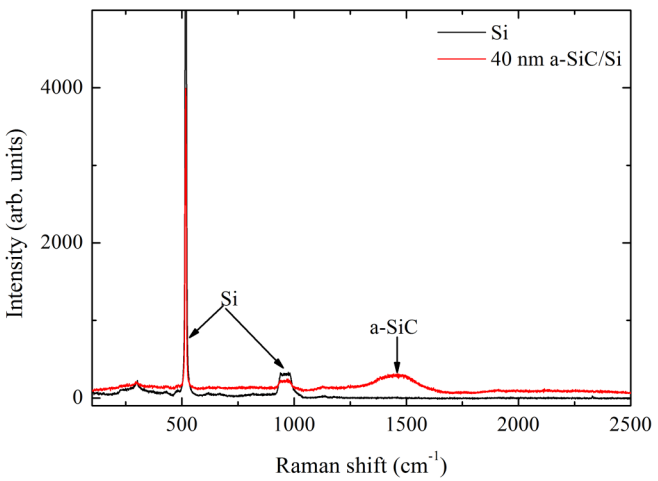

FIG. 1. Raman spectra of a bare silicon substrate and a 40 nm thick amorphous silicon carbide film on a silicon substrate. According to Ref. 28, the stoichiometric ratio in the deposited film is 1:1.

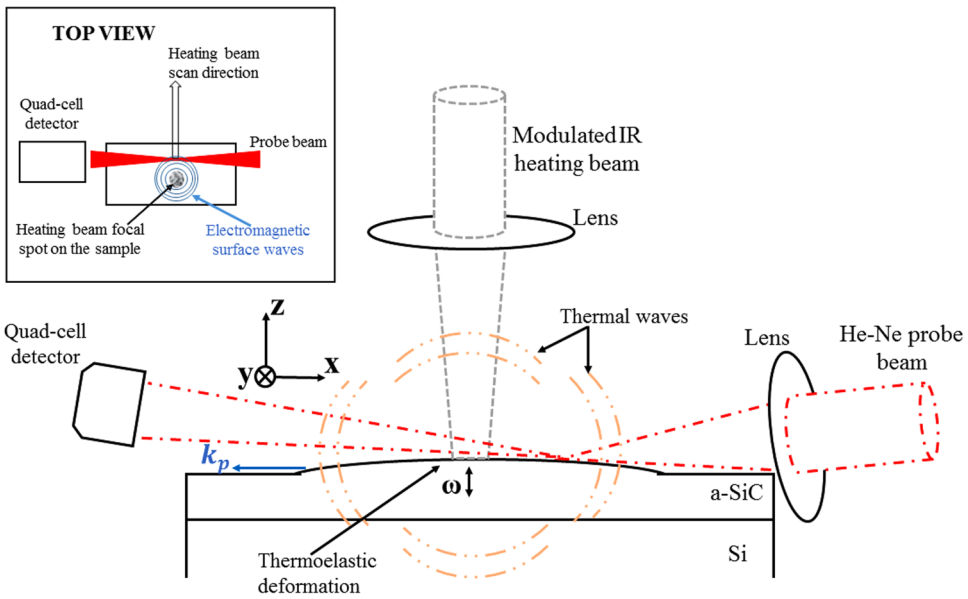

FIG. 2. Side view and top view of the experimental setup showing scattering of surface electromagnetic waves during thermoelastic deformation of the sample surface, the generation of thermal waves in the air and in the sample, and the detection of the generated thermal waves using the mirage effect. k_p is the wavevector of the scattered surface electromagnetic modes.

short-correlation structures, such as amorphous materials, the requirement of total momentum conservation for the interaction between MIR radiations and polar vibration modes breaks down.[30–32] Therefore, vibration modes whose frequencies match with that of incident MIR radiations may absorb a noticeable fraction of the heating beam irrespective of their wavevectors. Hence, breaking the moment conservation requirement increases the probability of optical absorption and allows for significant heating of the a-SiC film and, thus, a thermal excitation of the SPhP modes as well as the Zenneck and guided modes.[33] We will demonstrate the optical absorption of the incoming MIR light in the a-SiC layer later by the experimental results. All these thermally excited electromagnetic surface waves can contribute to thermal conduction in the plane of the measured sample. The high optical absorption of MIR radiations also leads to the occurrence of a periodic vertical surface displacement in the heated region.[29] Such an induced localized defect on the surface has proven to be efficient for launching the surface modes on the surface of the measured sample.[34]

Besides excitation and launching of electromagnetic surface modes, the modulated heating beam serves to generate rapidly damped thermal waves in and above the measured sample. These thermal waves give rise to periodic gradients of temperature and index of refraction in the air. These gradients are capable of periodically deflecting a He–Ne laser probe beam, passing very close to the surface, at the frequency of the modulation of the heating beam. In the used experimental setup, the probe beam is incident with an angle of 1° from the surface and focuses on the sample surface well before the heating spot. Hence, the angular deflection of the probe beam due to the mirage effect takes place after the reflection of the probe beam from the sample surface. Since the heating beam, the probe beam, and the sample normal are all in the same plane, the surface displacement may contribute only to the longitudinal component (along the z-axis) of the angular deflection of the probe beam. Therefore, to avoid contribution from surface displacement, we omit the longitudinal angular deflection and record only the transverse component (along the y-axis) of the angular deflection of the probe beam by using a four-quadrant photodetector. This experimental procedure has demonstrated efficacy in suppressing the effect of surface displacement on the recorded signal.[29] As we show in the inset of Fig. 2, to measure thermal diffusivity, we move the heating beam across the sample surface perpendicularly to the probe beam and record the angular deflection of the probe beam as a function of the offset distance between the heating beam and the probe beam. We repeat the measurement for different beam modulation frequencies to increase the accuracy of the analysis of the data. Then, we fit the experimental results to an anisotropic theory for the mirage effect considering a single-layer model. We note here that the generated thermal wave in the air dies out rapidly to zero.[35] Hence, its characteristic wavelength is almost equal to the thermal diffusion length, which is given by

$$L_{th} = \sqrt{\frac{\alpha_{s,y}}{\pi f}}, \tag{1}$$

where $\alpha_{s,y}$ is the in-plane thermal diffusivity of the measured sample and f is the heating beam modulation frequency. Since we modulate the heating beam at frequencies of the order of 1 kHz and typically $\alpha_{s,y}$ is about 1 cm^2/s, we estimate the wavelength of the generated thermal wave to be approximately 150 μm. This value is orders of magnitude larger than the thicknesses of the deposited a-SiC films. Therefore, the generated thermal wave is insensitive to the interface between the a-SiC film and the Si substrate. Consequently, a single layer model ignoring the scattering of thermal waves at interfaces is appropriate to describe the measured data.

III. RESULTS AND DISCUSSION

To identify the surface electromagnetic modes that efficiently contribute to heat transport in an a-SiC thin film, we deduced the mean-free-path of the SPhP modes of an a-SiC film of nanometric thickness deposited on a Si substrate by solving the SPhP dispersion relation,

$$\tanh(2p_1 d) = -\frac{p_1\varepsilon_1(\omega)(p_2\varepsilon_3 + p_3\varepsilon_2)}{p_1^2\varepsilon_2\varepsilon_3 + p_2p_3\varepsilon_1^2(\omega)}, \quad (2)$$

with considering a real wavenumber ω and a complex wavevector $q = q' + iq''$.[5] In Eq. (2), d and $\varepsilon_1(\omega)$ are the thickness and the complex dielectric function of the a-SiC film, respectively, ε_2 is the dielectric constant of Si, and ε_1 is the dielectric constant of the air. The parameters p_i have the dimension of a wavevector and are given by

$$p_i^2 = q^2 - \omega^2\varepsilon_0\mu_0\varepsilon_i, \quad (3)$$

where ω is the wavenumber. We deduced the complex dielectric function of a-SiC from the infrared reflectivity spectrum of a 600 nm thick a-SiC film deposited on Si. We present the real and imaginary parts of the complex dielectric function of a-SiC in Fig. 3. In the inset of Fig. 3, we show the infrared reflectivity spectrum from which the complex dielectric function of a-SiC is derived. Readers can find a detailed description of the numerical technique used to extract the complex dielectric function from the reflectivity measurement in Refs. 36 and 37. In Fig. 4, we present the function $q'(\omega)$, which determines the dispersion of the SPhP modes, and the inverse of the function $q''(\omega)$, which gives the mean-free-path of the SPhP modes. For comparison, we also present in Fig. 4 the dispersion and mean-free-path of the SPhP modes of crystalline SiC. The mean-free-path of the SPhP modes of crystalline SiC is generally larger than that of a-SiC. However, the SPhP modes of crystalline SiC exist only in the Reststrahlen band (i.e., in the spectral range between the transverse optical phonon frequency and the longitudinal phonon frequency at the center of the Brillouin zone), whereas the region of existence of the SPhP modes of a-SiC extends from q = 0 to q → ∞.[5] As shown in Fig. 4, all SPhP modes of a-SiC with frequencies above 1000 cm^{-1} can effectively contribute to heat transport because they are characterized by a mean-free-path of the order of a few tens of micrometers.

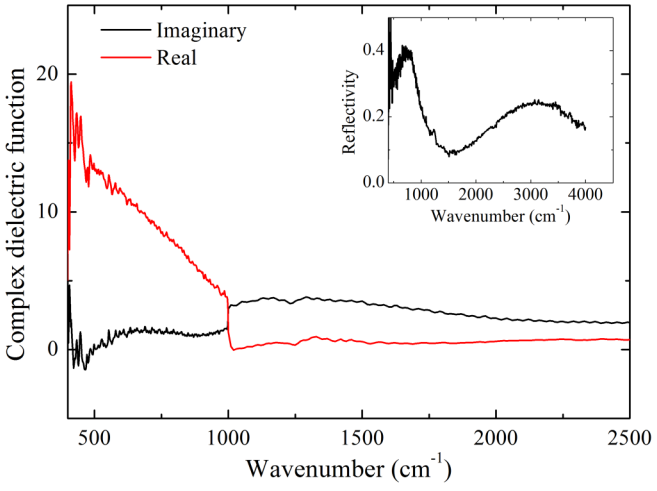

FIG. 3. The real and imaginary parts of the complex dielectric function of amorphous silicon carbide in the mid-infrared spectral range. The inset figure shows the reflectivity spectrum of a 600 nm thick amorphous silicon carbide film deposited on silicon from which the complex dielectric function is derived.

To evaluate the contribution of the surface electromagnetic modes of a-SiC to heat transfer, we have carried out MIR photothermal-beam-deflection measurements on the samples investigated by using the experimental setup described in Sec. II. We present in Figs. 5–8 the amplitudes and phases of the transverse signals obtained from a bare Si substrate, a 40 nm a-SiC film on Si, a 16 nm a-SiC film on Si, and a 3 nm a-SiC film on Si relative to the offset distance between the heating beam and the probe beam. The fact that the magnitudes of the signals from the samples with a-SiC films are higher than the signal from the bare Si substrate indicates that a noticeable amount of MIR radiations is absorbed and converted to heat in the a-SiC films. Thus, electromagnetic surface modes are thermally excited in the a-SiC films.

One can deduce the in-plane thermal diffusivity of the measured sample most accurately from the slope of the signal phase. As we turn the heating beam on, we deposit heat in the irradiated region at a rate determined by the modulation frequency of the heating beam. Then, the heat diffuses out from the center, and the peak signal occurs at a later time (a more negative signal phase) as the offset distance between the heating beam and the probe beam increases. Hence, there must be a direct relationship between the slope of the signal phase, the rate of heat transport in the plane of the sample (i.e., the in-plane thermal diffusivity), and the modulation frequency of the heating beam. For optically thin materials, as is the case of Si for optical excitation of a wavelength of 10.6 μm, experiments demonstrated that beyond the heating beam waist, the slope of the signal phase is approximately 0.925 rad/L_{th},[38] where the in-plane thermal diffusion length L_{th} is related to in-plane thermal diffusivity $\alpha_{s,y}$ and the heating beam modulation frequency f according to Eq. (1). This well-established technique for the analysis of the photothermal-beam-deflection signal allowed us to deduce the in-plane thermal diffusion lengths of the samples investigated at the four measured modulation frequencies from the slopes of the phases of the signals obtained from direct measurements. Then, as we show in Fig. 9(a), we plotted the squares of the obtained thermal diffusion lengths vs $1/\pi f$ for each sample and fitted the data points to straight lines passing through the origin. According to Eq. (1), the slopes of these straight lines provide the in-plane thermal diffusivities of the measured samples. We obtained the same value of in-plane thermal diffusivity for both the bare Si substrate and the 40 nm thick a-SiC film on Si. As can be noticed from Fig. 9(a), the obtained thermal diffusivity value for these two samples is in good agreement with previously reported values for thermal diffusivity of Si.[39] However, we found that the in-plane thermal diffusivity of the a-SiC/Si structure increases markedly with decreasing thickness of the a-SiC film. We found

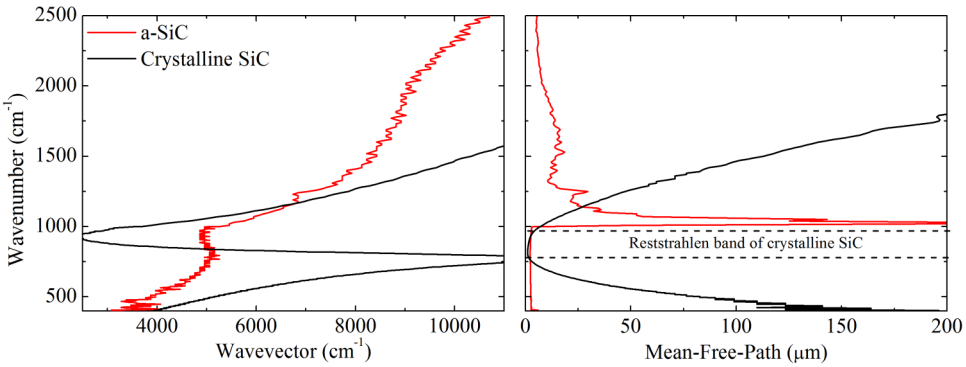

FIG. 4. Dispersion relation and mean-free-path of the SPhP modes of amorphous silicon carbide film of nanometric thickness deposited on a silicon substrate. The dispersion and mean-free-path of the SPhP modes of crystalline SiC are also plotted for comparison.

that the in-plane thermal diffusivity in the 3 nm a-SiC film on Si is larger than the thermal diffusivity of Si by a factor of approximately two. These results demonstrate substantial thermal diffusivity by surface electromagnetic waves and support the theoretical prediction that the decrease in thickness of the polar dielectric promotes the interaction between surface electromagnetic waves propagating on either side of it, which significantly improves thermal diffusivity in the sample plane.

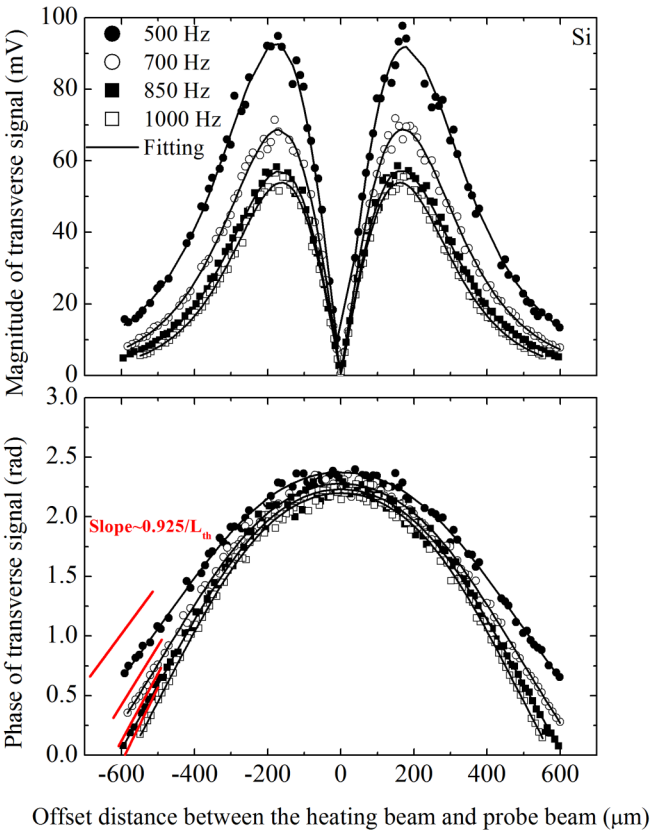

FIG. 5. Magnitude and phase of the transverse signals from a bare silicon substrate relative to the offset distance between the heating beam and the probe beam for four different heating beam modulation frequencies. The experimental data are shown using symbols. The fits of the experimental data to an anisotropic theory for the mirage effect are shown using solid lines.

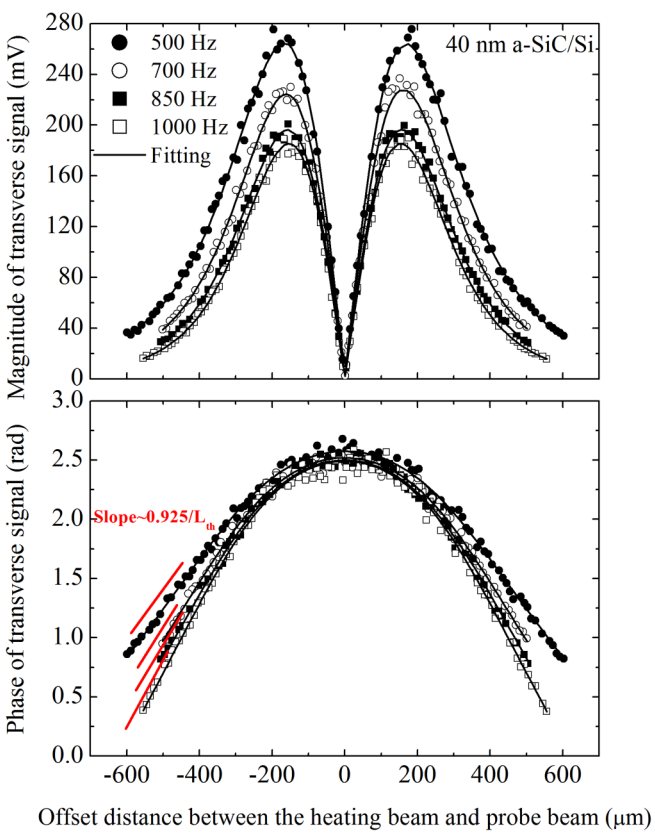

FIG. 6. Magnitude and phase of the transverse signals from a 40 nm a-SiC film on Si relative to the offset distance between the heating beam and the probe beam for four different heating beam modulation frequencies. The experimental data are shown using symbols. The fits of the experimental data to an anisotropic theory for the mirage effect are shown using solid lines.

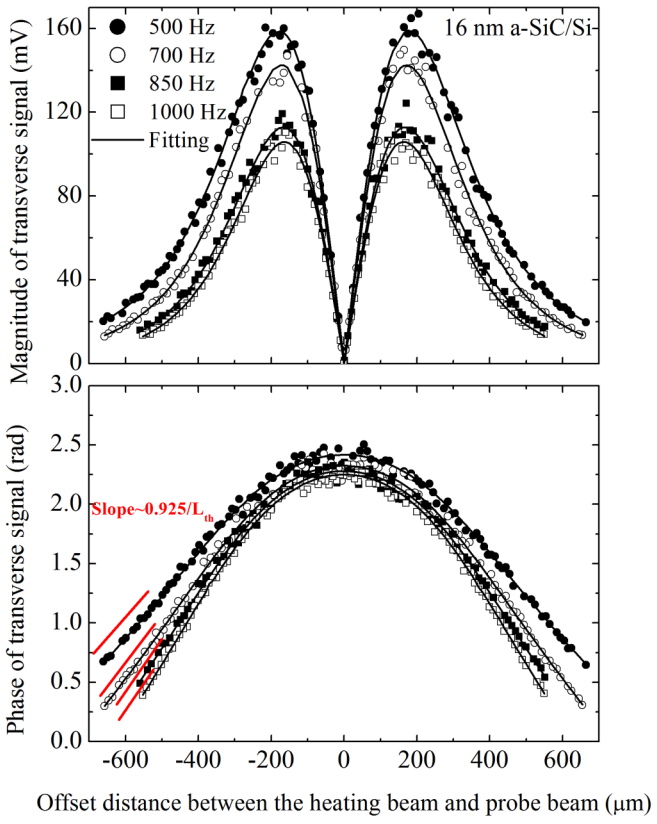

FIG. 7. Magnitude and phase of the transverse signals from a 16 nm a-SiC film on Si relative to the offset distance between the heating beam and the probe beam for four different heating beam modulation frequencies. The experimental data are shown using symbols. The fits of the experimental data to an anisotropic theory for the mirage effect are shown using solid lines.

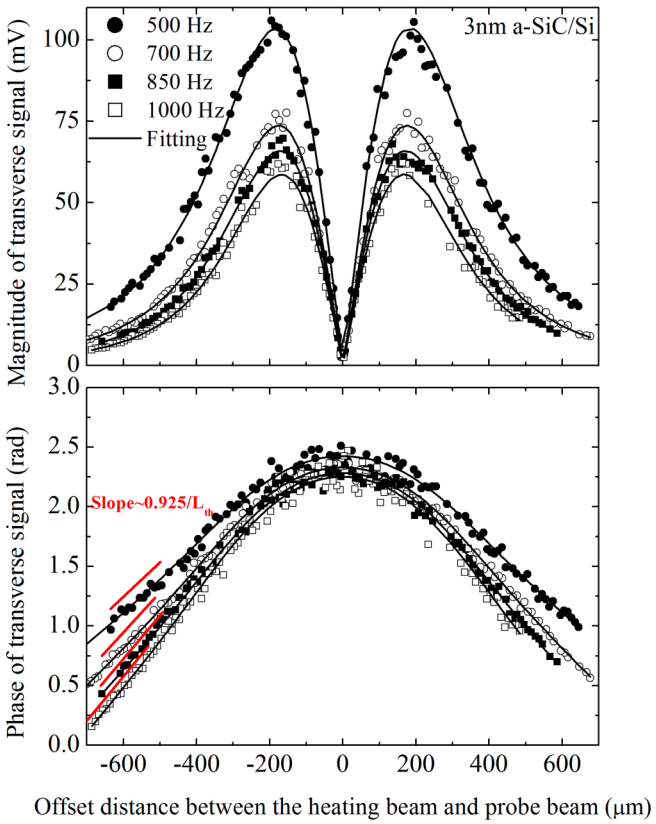

FIG. 8. Magnitude and phase of the transverse signals from a 3 nm a-SiC film on Si relative to the offset distance between the heating beam and the probe beam for four different heating beam modulation frequencies. The experimental data are shown using symbols. The fits of the experimental data to an anisotropic theory for the mirage effect are shown using solid lines.

We also have deduced the in-plane thermal diffusion lengths of the samples investigated at four measured modulation frequencies by fitting the magnitudes and phases of the recorded transverse signals to a formalism for the mirage effect that takes into account the anisotropic thermal transport in the measured medium. As demonstrated in Ref. 29, when we focus a probe beam incident at a grazing angle (~1° from the sample surface) on the sample surface, the mirage effect governs the transverse component of vector angular deflection, and we can express the transverse angular deflection as

$$M_{trans} = \frac{-1}{\pi}\frac{1}{n}\frac{dn}{dT}e^{-q_g^2R_2^2/4}\int_0^\infty dk\frac{k_g cos(ky)e^{ik_g h}e^{-k^2R_1^2/4}}{(\kappa_{s,z}k_s + \kappa_g k_g)}, \quad (4)$$

where y is the offset distance between the heating beam and the probe beam, the subscript z indicates parameters defined in the direction perpendicular to the surface, n is the index of refraction of the air, R_1 is the radius of the heat spot on the sample surface, R_2 is the radius of the probe beam above the heated region, h is the height of the probe beam from the surface, q is the cross-plane thermal conductivity of the sample, and $\kappa_{s,z}$ is the thermal conductivity of the air. The thermal wavevector in the sample is defined as

$$k_s = \left(q_s^2 - \frac{L_{th}^2}{L_{th,z}^2}k^2\right)^{\frac{1}{2}}. \quad (5)$$

It provides the dependence of transverse angular deflection on the cross-plane thermal diffusion length $L_{th,z}$ and the in-plane thermal diffusion length L_{th}.[29] The thermal wavenumber q_s is related to the cross-plane thermal diffusion length according to

$$q_s = (1+i)\left(\frac{1}{L_{th,z}}\right). \quad (6)$$

The thermal wavevector in the air is given by

$$k_s = (q_g^2 - k^2)^{\frac{1}{2}}, \quad (7)$$

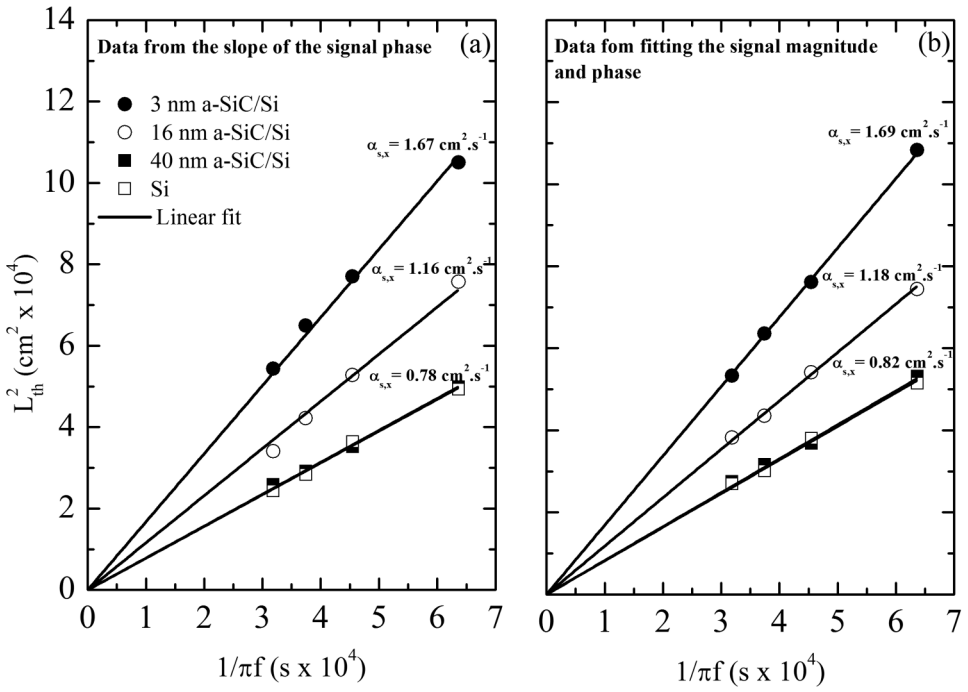

FIG. 9. The squares of the in-plane thermal diffusion length in the samples investigated vs $1/\pi f$, where f is the heating beam modulation frequency. Each set of data points is fitted to a straight line whose slope is equal to the in-plane thermal diffusivity of the corresponding sample. (a) Data points obtained from the analysis of the slopes of the phases of the measured signals. (b) Data points obtained from fitting the magnitudes and phases of the measured signals to a formalism for the mirage effect that accounts for the anisotropy of thermal transport in the measured sample.

where

$$q_g = (1+i)\left(\frac{\Omega}{2\alpha_g}\right)^{\frac{1}{2}}. \tag{8}$$

Here, Ω is the angular modulation frequency and α_g is the thermal diffusivity of the air. To reduce the number of the model adjustable parameters, we measured the radius of the probe beam R_2using the knife-edge method. Moreover, we estimated R_1 by using the fact that for the measured heating beam modulation frequencies, the theory of photothermal-beam-deflection predicts that the maximum of the signal magnitude occurs at $r = 1.1 \times R_1$.[40] Furthermore, for all the samples investigated, we set the cross-plane thermal diffusion length $L_{th,z}$ equal to the thermal diffusion length of Si at the measured frequency because the electromagnetic surface modes do not contribute to heat transport in the direction perpendicular to the surface. Thus, the only adjustable parameters were the height of the probe beam above the surface h, the radius of the heat spot on the sample R_1, and the in-plane thermal diffusion length L_{th}. We illustrate in Figs. 5–8 the high quality of the multi-parameter least-squares fits of the magnitudes and phases of the signals from the bare Si substrate and the samples supporting surface electromagnetic waves. We present in Fig. 9(b) the squares of the obtained diffusion lengths vs $1/\pi f$. We fitted the data points in Fig. 9(b) to straight lines passing through the origin to deduce the in-plane thermal diffusivities of the measured samples. We obtained results in satisfactory agreement with those obtained from the analysis of the slopes of the phases of the measured signals. In Fig. 10, we show the results for the in-plane thermal diffusivities of the measured samples obtained by fitting the experimental data to the theory of the mirage effect and from the analysis of the slopes of the phases of the signals. Although the results deduced from the two different analysis techniques show a discrepancy of ~5%, they both demonstrate a substantial enhancement in the in-plane

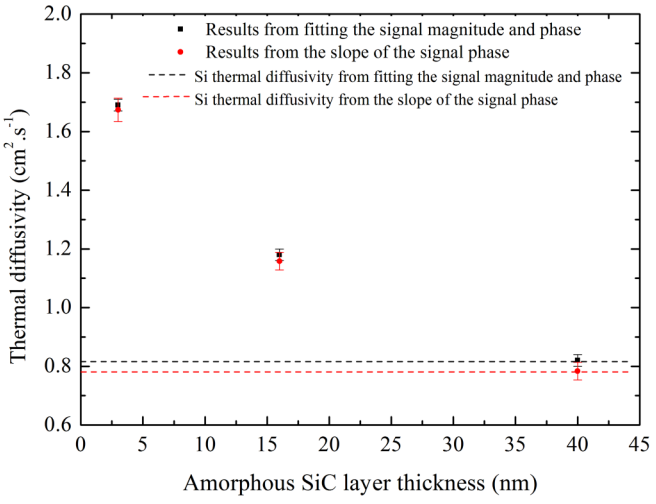

FIG. 10. In-plane thermal diffusivity vs the thickness of the a-SiC film as obtained from fitting the experimental data to an anisotropic formalism for the mirage effect and from the analysis of the slopes of the phases of the measured signals. The uncertainties are determined by the scatter in the data points.

thermal diffusivity as the thickness of the a-SiC film deposited on Si decreases.

The measurement analysis presented above shows that the in-plane thermal diffusivity of the 3 nm thick a-SiC film on Si is almost twice the thermal diffusivity of Si. Since the total in-plane heat flow rate in this sample is the sum of the heat flow rate due to the surface electromagnetic waves of the a-SiC film $\left(\frac{\Delta Q}{\Delta t}\right]_{SEMW}\right)$ and the heat flow rate due to phonons in the Si substrate $\left(\frac{\Delta Q}{\Delta t}\right]_{Phonon}\right)$, we can write as

$$\frac{\Delta Q}{\Delta t}\Big]_{SEMW} \approx \frac{\Delta Q}{\Delta t}\Big]_{Phonon}. \tag{9}$$

On the other hand, the in-plane heat flow rate is directly proportional to the in-plane thermal diffusivity times the thickness of the material. As the Si substrate is several orders of magnitude thicker than the a-SiC film, Eq. (9) indicates that thermal diffusivity by electromagnetic surface waves in the 3 nm thick a-SiC film is orders of magnitude larger than thermal diffusivity by phonons in Si. This result draws an analogy between tunneling of electromagnetic surface waves between polar dielectrics that demonstrated orders of magnitude enhancement of thermal radiation in the near-field limit and the interaction between electromagnetic surface waves propagating on either side of a polar dielectric that leads to orders of magnitude enhancement in thermal conduction.

IV. CONCLUSION

We used a photothermal-beam-deflection technique with a modulated mid-infrared heating source to excite and launch surface electromagnetic waves onto the surfaces of an amorphous silicon carbide film deposited on silicon and generate periodic temperature and refractive index gradients above the sample surface. These gradients are capable of periodically deflecting a He–Ne laser probe beam, passing very close to the surface, at the frequency of the modulation of the heating beam. Then, we fitted the measured probe beam deflections to an analytical model for the mirage effect that takes into account the thermal anisotropy of the measured sample to deduce the contribution of the excited surface electromagnetic waves to in-plane thermal diffusivity of the sample. We analyzed the experimental data obtained from samples with amorphous silicon carbide films of different thicknesses using two different approaches. We found that in-plane thermal diffusivity by surface electromagnetic modes becomes pronounced for ultra-thin films of amorphous silicon carbide and increases rapidly as the film thickness decreases. We attributed these results to the fact that the reduction in the thickness of the amorphous silicon carbide film promotes the interaction between the surface electromagnetic waves propagating on either side of the film, which significantly enhances thermal diffusivity in the plane of the measured sample. We have also demonstrated the analogy between the substantial enhancement in thermal radiation in the near-field limit resulting from tunneling of surface electromagnetic waves between polar dielectrics and the substantial enhancement in thermal conduction resulting from an interaction between surface electromagnetic waves propagating on either side of a polar dielectric.

ACKNOWLEDGMENTS

The authors gratefully acknowledge financial support by Munib and Angela Masri Institute of Energy and Natural Resources and the American University of Beirut Research Board (URB).

DATA AVAILABILITY

The data that support the findings of this study are available from the corresponding author upon reasonable request.

REFERENCES

[1]A. I. Boukai, Y. Bunimovich, J. Tahir-Kheli, J.-K. Yu, W. A. Goddard III, and J. R. Heath, Nature **451**, 168 (2008).
[2]A. I. Hochbaum, R. Chen, R. D. Delgado, W. Liang, E. C. Garnett, M. Najarian, A. Majumdar, and P. Yang, Nature **451**, 163 (2008).
[3]B. L. Davis and M. I. Hussein, Phys. Rev. Lett. **112**, 055505 (2014).
[4]A. Iskandar, A. Gwiazda, Y. Huang, M. Kazan, A. Bruyant, M. Tabbal, and G. Lerondel, J. Appl. Phys. **120**, 095106 (2016).
[5]I. Prigogine and S. A. Rice, *Aspects of the Study of Surfaces* (John Wiley & Sons, 1974), Vol. 27, p. 355.
[6]J. D. Caldwell, L. Lindsay, V. Giannini, I. Vurgaftman, T. L. Reinecke, S. A. Maier, and O. J. Glembocki, Nanophotonics **4**, 44 (2015).
[7]C. F. Bohren and D. R. Huffman, *Absorption and Scattering of Light by Small Particles* (Wiley-VCH, Weinheim, 1998), p. 241.
[8]M. Francoeur, *Near-Field Radiative Transfer: Thermal Radiation, Thermophotovoltaic Power Generation and Optical Characterization* (University of Kentucky, 2010).
[9]K. Joulain, J.-P. Mulet, F. Marquier, R. Carminati, and J.-J. Greffet, Surf. Sci. Rep. **57**, 59 (2005).
[10]R. Baltaji and M. Kazan, J. Appl. Phys. **125**, 065102 (2019).
[11]S. Inampudi and H. Mosallaei, Phys. Rev. B. **96**, 125407 (2017).
[12]M. Francoeur, M. P. Mengüç, and R. Vaillon, Appl. Phys. Lett. **93**, 043109 (2008).
[13]Y. Miyoshi, Y. Fukazawa, Y. Amasaka, R. Reckmann, T. Yokoi, K. Ishida, K. Kawahara, H. Ago, and H. Maki, Nat. Commun. **9**, 1279 (2018).
[14]K. Kim, B. Song, V. Fernández-Hurtado, W. Lee, W. Jeong, L. Cui, D. Thompson, J. Feist, M. T. H. Reid, F. J. García-Vidal, J. C. Cuevas, E. Meyhofer, and P. Reddy, Nature **528**, 387 (2015).
[15]B. Song, D. Thompson, A. Fiorino, Y. Ganjeh, P. Reddy, and E. Meyhofer, Nat. Nanotechnol. **11**, 509 (2016).
[16]B. Song, Y. Ganjeh, S. Sadat, D. Thompson, A. Fiorino, V. Fernández-Hurtado, J. Feist, F. J. Garcia-Vidal, J. C. Cuevas, P. Reddy, and E. Meyhofer, Nat. Nanotechnol. **10**, 253 (2015).
[17]D.-Z. A. Chen, A. Narayanaswamy, and G. Chen, Phys. Rev. B **72**, 155435 (2005).
[18]J. Ordonez-Miranda, L. Tranchant, K. Joulain, Y. Ezzahri, J. Drevillon, and S. Volz, Phys. Rev. B **93**, 035428 (2016).
[19]D.-Z. A. Chen and G. Chen, FHMT **1**, 023005 (2010).
[20]J. Ordonez-Miranda, L. Tranchant, B. Kim, Y. Chalopin, T. Antoni, and S. Volz, Phys. Rev. Lett. **112**, 055901 (2014).
[21]A. M. Hofmeister, J. Dong, and J. M. Branlund, J. Appl. Phys. **115**, 163517 (2014).
[22]T. Tokunaga, L. Tranchant, N. Takama, S. Volz, and B. Kim, J. Phys. Conf. Ser. **395**, 012108 (2012).
[23]E. J. Tervo, O. S. Adewuyi, J. S. Hammonds, Jr., and B. A. Cola, Mater. Horiz. **3**, 434 (2016).
[24]L. Tranchant, S. Hamamura, J. Ordonez-Miranda, T. Yabuki, A. Vega-Flick, F. Cervantes-Alvarez, J. J. Alvarado-Gil, S. Volz, and K. Miyazaki, Nano Lett. **19**, 6924 (2019).
[25]P. Li, X. Yang, T. W. W. Maß, J. Hanss, M. Lewin, A.-K. U. Michel, M. Wuttig, and T. Taubner, Nat. Mat. **15**, 870 (2016).

[26]A. M. Dubrovkin, B. Qiang, H. N. S. Krishnamoorthy, N. I. Zheludev, and Q. J. Wang, Nat. Commun. **9**, 1762 (2018).
[27]A. M. Dubrovkin, B. Qiang, T. Salim, D. Nam, N. I. Zheludev, and Q. J. Wang, Nat. Commun. **11**, 1863 (2020).
[28]Y. Inoue, S. Nakashima, A. Mitsuishi, S. Tabata, and S. Tsuboi, Solid State Commun. **48**, 1071 (1983).
[29]J. Younes, Z. Harajli, M. Soueidan, D. Fabrègue, Y. Zaatar, and M. Kazan, J. Appl. Phys. **127**, 173101 (2020).
[30]R. Shuker and R. W. Gammon, Phys. Rev. Lett. **25**, 222 (1970).
[31]K. K. Tiong, P. M. Amirtharaj, F. H. Pollak, and D. E. Aspnes, Appl. Phys. Lett. **44**, 122 (1984).
[32]A. Iskandar, A. Gwiazda, J. Younes, M. Kazan, A. Bruyant, M. Tabbal, and G. Lerondel, Phys. Rev. B **97**, 094308 (2018).
[33]S. Gluchko, B. Palpant, S. Volz, R. Braive, and T. Antoni, Appl. Phys. Lett. **110**, 263108 (2017).
[34]S. Dai, Q. Ma, Y. Yang, J. Rosenfeld, M. D. Goldflam, A. McLeod, Z. Sun, T. I. Anderson, Z. Fei, M. Liu, Y. Shao, K. Watanabe, T. Taniguchi, M. Thiemens, F. Keilmann, P. Jarillo-Herrero, M. M. Fogler, and D. N. Basov, Nano Lett. **17**, 5285 (2017).
[35]A. Mandelis, *Photoacoustic and Thermal Wave Phenomena in Semiconductors* (Elsevier Science Publishing Co., 1987).
[36]A. Al Mohtar, M. Kazan, T. Taliercio, L. Cerutti, S. Blaize, and A. Bruyant, Nanotechnology **28**, 125701 (2017).
[37]N. Rahbany, M. Kazan, M. Tabbal, R. Tauk, J. Jabbour, J. Brault, B. Damilano, and J. Massies, J. Appl. Phys. **114**, 053505 (2013).
[38]M. A. Olmstead, N. M. Amer, S. Kohn, D. Fournier, and A. C. Boccara, Appl. Phys. A Solids Surf. **32**, 141 (1983).
[39]H. R. Shanks, P. D. Maycock, P. H. Sidles, and G. C. Danielson, Phys. Rev. **130**, 1743 (1963).
[40]J. Opsal, A. Rosencwaig, and D. L. Willenborg, Appl. Opt. **22**, 3169 (1983).